

# PillarTrack: Redesigning Pillar-based Transformer Network for Single Object Tracking on Point Clouds

Weisheng Xu<sup>1†</sup>, Sifan Zhou<sup>2†\*</sup>, Zhihang Yuan<sup>3</sup>

**Abstract**—LiDAR-based 3D single object tracking (3D SOT) is a critical issue in robotics and autonomous driving. It aims to obtain accurate 3D BBox from the search area based on similarity or motion. However, existing 3D SOT methods usually follow the point-based pipeline, where the sampling operation inevitably leads to redundant or lost information, resulting in unexpected performance. To address these issues, we propose PillarTrack, a pillar-based 3D single object tracking framework. Firstly, we transform sparse point clouds into dense pillars to preserve the local and global geometrics. Secondly, we introduce a Pyramid-type Encoding Pillar Feature Encoder (PE-PFE) design to help the feature representation of each pillar. Thirdly, we present an efficient Transformer-based backbone from the perspective of modality differences. Finally, we construct our PillarTrack tracker based above designs. Extensive experiments on the KITTI and nuScenes dataset demonstrate the superiority of our proposed method. Notably, our method achieves state-of-the-art performance on the KITTI and nuScenes dataset and enables real-time tracking speed. We hope our work could encourage the community to rethink existing 3D SOT tracker designs.

## I. INTRODUCTION

3D Single object tracking (3D SOT) has a diverse applications in autonomous driving and robotics. Given the initial state (appearance and location) of specific target in the first frame, 3D single object tracking aims to estimate its 3D state across subsequent frames. Existing LiDAR-based 3D single object tracking methods [1]–[7] generally follow the Siamese paradigm from 2D visual object tracking, aiming to achieve a trade-off between runtime and accuracy. Given the sparse and irregular input point cloud, these methods initially leverage PointNet families [8], [9] to learn point-wise discriminative representation, and then obtain point-wise similarity with a feature aggregation module. Finally, they estimate the state of specific targets based on these similarity features. SC3D [10] stands as the pioneering LiDAR-based 3D Siamese tracker, leveraging an efficient auto-encoder based on PointNet [11] for point-wise feature encoding. Subsequently, approaches such as P2B [2], 3D-SiamRPN [1], BAT [4] and PTT [3], [12] employ PointNet++ [9] to extract more effective point-wise representation and achieve superior tracking performance. However, one common issue with above point-based 3D SOT methods is the need for re-sampling the input points to a fixed number. For instance, P2B [2] requires

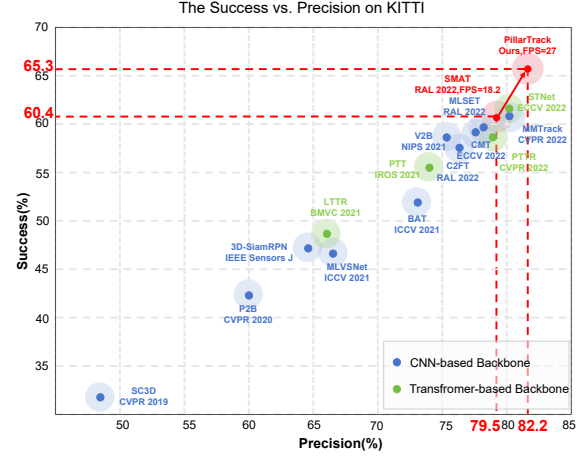


Fig. 1: Comparison with other 3D SOT methods on KITTI dataset. We categorize methods based on the Backbone architecture and report their performance on Success and Precision.

the input points to be re-sample to 1024 for the search area and 512 for the template point cloud in order to align the network input. This re-sample operation inevitably introduces the potential for redundant or lost information, which can adversely affect performance. Additionally, the reliance on point query/retrieval in 3D space (e.g., PointNet++ [9]) for the re-sampling process may not be friendly to efficient hardware implementation.

To this end, inspired by the recent advancements in pillar-based 3D object detectors [13]–[15] due to their real-time speed and high performance. Therefore, we convert the sparse and irregular point clouds into dense and regular pillar representations. It is noteworthy that the 3D SOT task can be regarded as a specific 3D object detection task within a local search area, with the additional template point prior information. Therefore, it is natural to leverage advanced principles from 3D point cloud detection to improve point cloud tracking tasks. Specifically, pillar-based point cloud representation possesses following advantages: (1) Pillar representation is dense and ordered, facilitating seamless integration with advanced 2D image-based techniques without much modification. (2) The compact nature of the pillar representation reduces computational overhead while maintaining a desirable trade-off between performance and speed. (3) Pillar representation is deployment-friendly, making it highly suitable for resource-limited devices like mobile robots or drones. Particularly, pillar representation naturally aligns with the high demanding real-time requirements of 3D trackers,

<sup>1</sup>Weisheng Xu is with the School of Mathematics and Computer Science, Nanchang University, Nanchang 330031, China. 6105121101@email.ncu.edu.cn, <sup>2</sup>Sifan Zhou is with the School of Automation, Southeast University, Nanjing 210096, China. sifanjay@gmail.com, <sup>3</sup>Zhihang Yuan is with Houmo AI, Beijing 100088, China. hahnyuan@gmail.com

<sup>†</sup> Authors with equal contribution. \* Corresponding author.

making it well-suited for tracking tasks.

Currently, few works [16], [17] are dedicated to pillar-based 3D SOT with point clouds. SMAT [16] addresses this gap by transforming sparse 3D point clouds into dense pillars and then utilizing a transformer-based encoder for multi-scale feature extraction and interaction, yielding promising results. However, SMAT directly adopts a simplistic pillar encoding module from PointPillars [18] limits the quality of the pillar representations. Besides, their backbone directly follows the design principle of vision transformers tailored for RGB image, which may be sub-optimal for point cloud modalities. PTTR++ [17] introduces a fusion of point-wise and pillar-wise views to further enhance the performance of PTTR [6]. Nevertheless, PTTR++ still involves a re-sampling operation within its pipeline, which presents paratical deployment challenges.

In this paper, we propose PillarTrack, a pillar-based 3D single-object tracking framework, aiming to improve tracking performance while enhancing the inference speed. Firstly, we transform sparse and unordered point clouds into dense and regular pillar representations to reduce information loss caused by re-sampling operation and propose a Pyramid-type Encoding Pillar Feature Encoder (PE-PFE) design to help the feature learning of each pillar. Secondly, we argue the design of existing Transformer-based backbone from the perspective of modality differences and propose an modality-aware Transformer-based backbone specifically tailored for point cloud modalities, achieving higher performance with fewer GFLOPs. Finally, we construct our PillarTrack network. Extensive experiments on the KITTI and nuScenes dataset demonstrate the superiority of our proposed method. As shown in Figure 1, our approach achieves state-of-the-art performance on the KITTI and nuScenes dataset, striking a better balance between speed and accuracy, and catering to diverse practical needs. In conclusion, the main contributions of this paper are as follows:

- **PE-PFE:** A Pyramid-type Encoding Pillar Feature Encoder (PE-PFE) design to encode the point coordinate of each pillar with pyramid-type representation, and bring the performance gain without extra computational overhead.
- **Modality-aware Transformer-based Backbone:** A more suitable for point cloud modalities, aiming to enhance feature representation. This design involves a simple adjustment of computational resources allocated to the front-end of the backbone, allowing for capturing more semantic details of the input point cloud.
- **SOTA and Open-source:** Experiments on KITTI and nuScenes dataset show our method achieve the state-of-the-art performance. Besides, we will open source our code to the research community in <https://github.com/StiphyJay/PillarTrack>.

## II. RELATED WORK

### A. Single Object Tracking on Point Clouds

Benefiting from the nature of LiDAR that are less sensitive to illumination changes and capture accurate distance information, numerous works [1], [2], [4], [10], [19]–[22]

in LiDAR-based 3D Single Object Tracking (3D SOT) have merged. SC3D [10] leverages the Kalman filter for proposals generation and select the most suitable candidate based on Siamese network [23]. 3D-SiamRPN [1] combines 3D Siamese network with 3D RPN network for object tracking. P2B [2] introduces target-specific features and utilizes VoteNet [24] to estimate target center. Based on the P2B pipeline, BAT [4] incorporated Box-aware information to enhance similarity feature. Besides, V2B [22] introduces Voxel-to-BEV network for pixel-wise regression of 3D targets, M2-Track [21], [25] adopts a motion-centric paradigm to address the issue of 3D SOT and achieves remarkable performance. Inspired by the success of transformers [26], several methods [3], [5]–[7], [12], [27]–[29] have merged. PTT [3], [12] proposed Point-Track-Transformer module to assign weights to crucial point cloud features. LTTR [5] proposes a Transformer-based feature fusion module to learn semantic context among different region. PTTR [6] employs an attention-based feature matching mechanism to integrate target clues in similarity. STNet [7] develops an iterative coarse-to-fine correlation network for robust correlation learning. CXTrack [29] adopts transformer to extract richer contextual information from consecutive frames, enhancing localization accuracy. Recently, SMAT [16] encodes global similarity based on attention in the BEV to alleviate the impact of point sparsity. However, their backbone still partially inherits the design principles from ResNet [30] tailored for the image modality, which may be sub-optimal for point clouds modality.

### B. Pillar-based Object Detection on Point Clouds

Grid-based point cloud 3D detectors [13]–[15], [18], [31] generally transform unordered points into regular pillar/voxel and then utilize 2D/3D CNN to learn representation. VoxelNet [32] stands as a pioneering work that leverages Voxel Feature Extractor (VFE) and 3D CNN for 3D object detection. Subsequently, SECOND [33] employs 3D sparse convolution on non-empty voxels to accelerate training and inference. Different from above approaches, PointPillars [18] innovatively converts point clouds into pillars and leverages 2D CNN to enhance detection speed. After that, CenterPoint [31] proposes a center-based head design, achieving milestone performance. Furthermore, PillarNet [13] improves the accuracy of pillar-based 3D detectors through an “encoder-neck-head” architecture, achieving superior performance while maintaining real-time speed. Based on PillarNet [13], FastPillars [14] proposes a backbone design suitable for point cloud modality and considers deployment-friendly ability, resulting in new state-of-the-art. The success of these pillar-based 3D detectors greatly motivates us to explore the potential of simple pillar-based representation in 3D SOT tasks.

### C. Vision Transformer

Transformer [26] is first proposed in natural language processing (NLP). Subsequently, owing to its remarkable

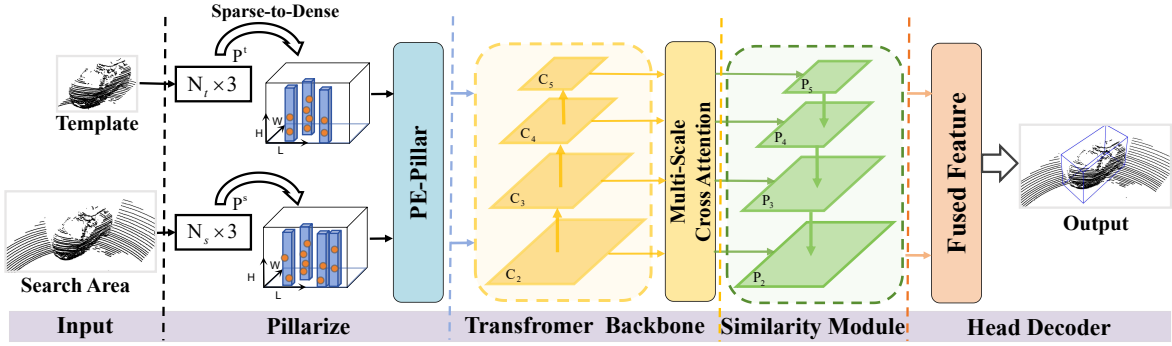


Fig. 2: The architecture of our PillarTrack network. Given the template and search area, we first use PE-Pillar to extract multi-scale features respectively. Then, MAE computes similarity by attention at each feature scale and then fuses the multi-scale similarity feature. Finally, we apply the detection head on the feature fusion map to localize the target.

ability for global modeling, the Transformer has shown significant success in image recognition tasks. ViT [34] leverage the Transformer structure to classify images by splitting them into patches. SwinTransformer [35] proposes a shifted windows attention mechanism, achieving excellent performance across various image tasks. PVT [36] and PVTv2 [37] utilize a progressive shrinking pyramid to construct a visual Transformer backbone. In the 3D Vison, Point Transformer [38] introduces a specialized Point Transformer layer tailored for processing unordered point clouds. PCT [39] utilizes 3D coordinates of points to generate position embedding and employs an attention module to extract point features from local neighborhoods. These efforts showcase outstanding performance in point cloud shape classification or part segmentation. For LiDAR-based 3D detection tasks, recent approaches [40], [41] first transform point clouds into regular pillars/voxels and then utilize dynamic sparse windows on BEV feature for feature extraction, yielding remarkable performance. In contrast, we employ the Transformer for global modeling on the pillarized feature, aiming to explore the potential of the Transformer in the object tracking task from a BEV perspective.

### III. PRELIMINARY

#### A. Problem Statement

In the task of the 3D Single Object Tracking (3D SOT), we initially define target point cloud (i.e., template)  $\mathbf{P}_t = \{\mathbf{p}_{ti} = [x_i, y_i, z_i, r_i]^T \in \mathbb{R}^{N \times 4}\}$ , where  $x_i, y_i, z_i$  denote the coordinate values of each point along the axes X, Y, Z, respectively, and  $r_i$  represents the laser reflection intensity. Our goal is to locate the 3D bounding box (3D BBox) of this target in the search area  $\mathbf{P}_s = \{\mathbf{p}_{si} = [x_j, y_j, z_j, r_j]^T \in \mathbb{R}^{M \times 4}\}$  frame by frame. Here,  $N$  and  $M$  is the number of points in target and search area. The 3D BBox is represented as  $\mathbf{B} = \{\mathbf{b} = [x, y, z, h, w, l, \theta]^T \in \mathbb{R}^{1 \times 7}\}$ , The coordinates  $x, y, z$  indicate the object's center, while  $h, w, l$  denote its size,  $\theta_j$  is the object's heading angle. Since the target's 3D BBox is known in the first frame, we need to regress the target center and heading angle in subsequent frames. By applying the displacement

and heading angle from the previous frame's 3D BBox, we can locate the target in the current frame.

#### B. Baseline Architecture Overview

As SMAT represents the first attempt at a pillar-based 3D Siamese tracker and has shown promising performance, we choose SMAT as our baseline and provide a brief overview of its structure. The core components of SMAT include: **1)** a naive pillar feature encoding module derived from Pointpillars, which transforms raw point cloud data into a pseudo-image; **2)** a Transformer-based backbone network that computes similarity through a multi-head attention mechanism for the multi-scale features from both the template and search branches, capturing local and global information within the point cloud; **3)** a neck module that integrates features from different scales and fuses multi-scale similarity features, enhancing the model's perception of multi-scale information; **4)** a decoder that predicts the position and orientation of the target object. These carefully designed features enable SMAT to effectively handle sparse point cloud data, offering an efficient solution for 3D Single Object Tracking.

#### C. Motivation

Our research endeavors to investigate a real-time, high-performance, pillar-based approach for 3D single-object tracking. To achieve this, we leverage the compact pillar representation and design a strong Transformer-based backbone that enhances pillar feature representation with reduced computational resources from the perspective of modality differences. Regarding the feature integration and similarity computation module, we follow the original design of baseline method [16], which has shown remarkable efficacy. We hope that our design principles offer a novel perspective in 3D single object tracking, encouraging the community to revisit existing methodologies.

### IV. METHOD

#### A. Pyramid-Encoded Pillar Feature Encoding Design

In pillar-based 3D detection methods [13], [14], [18], Pillar Feature Encoding (PFE) plays a crucial role, directly impacting the representation learning of BEV feature and

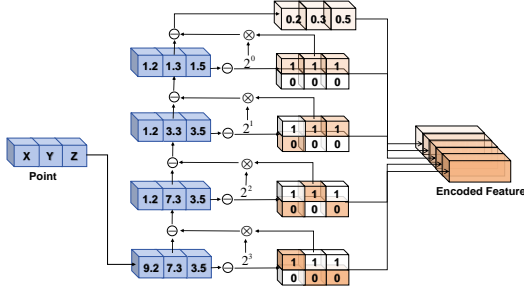


Fig. 3: The illustration of PE-PillarVFE design. We encode the channel information of the input point cloud in a pyramid-type fashion. This Pyramid-type encoding design allows the network to optimize more effectively without the input information loss.

final detection accuracy. Its significance extends to 3D single object tracking tasks as well. In SMAT, they utilize the PFE module from PointPillars [18] to extract pillar-wise feature. Here, taking PFE module as an example, we illustrate the details of their input encoding. The points in each pillar are initially concatenated along the channel dimension to form  $\hat{p}_i = \{[x_i, y_i, z_i, r_i, x_i^m, y_i^m, z_i^m, x_i^c, y_i^c, z_i^c] \in \mathbb{R}^{N_i \times 10}\}$ , where  $[x_i, y_i, z_i]$  is the original point coordinates in the ego frame,  $[x_i^m, y_i^m, z_i^m]$  denotes the offset of  $p_i$  from the mean of the xyz coordinates of all points within the current pillar, and  $[x_i^c, y_i^c, z_i^c]$  is the offset of  $p_i$  from the current pillar center. However, there exist significant numerical differences in the point-wise feature. For example, the numerical range of the  $[x_i, y_i, z_i]$  is  $[-3.2, 3.2]$  (i.e., the range of search area). However, the numerical range of  $[x_i^m, y_i^m, z_i^m]$  and  $[x_i^c, y_i^c, z_i^c]$  is  $[-0.1, 0.1]$ , since they are relative offset within a pillar. It can be observed that there exist significant numerical differences (almost  $30 \times$ ) between the point-wise feature channels in PFE. Such huge disparities in input values pose significant challenges for network optimization [42], [43]. Therefore, we propose a Pyramid-type Encoding Pillar Feature Encoder (PE-PFE) design aimed at reducing the numerical differences between the input channels, enabling the network towards better optimization on numerically stable inputs.

TABLE I: Tracking performance comparison of different PFE designs in the Car category in KITTI.

PFE Method	Success	Precision
PFE (SMAT [16] <sup>4</sup> )	68.9	79.6
PE-PFE(Ours)	70.8 (+1.9)	80.3 (+0.7)

As shown in Figure 3, we encode the channel values of the input point cloud in a pyramid-type manner, and finally retain a residual value that cannot be evenly divided. The encoding values from each layer and the residual value are then cascaded together as point-wise features, which are then processed by the PFE module. It is important to note that this pyramid-type encoding design significantly reduces the nu-

<sup>4</sup>The model was trained on a setup comprising four NVIDIA GeForce RTX 3090 GPUs

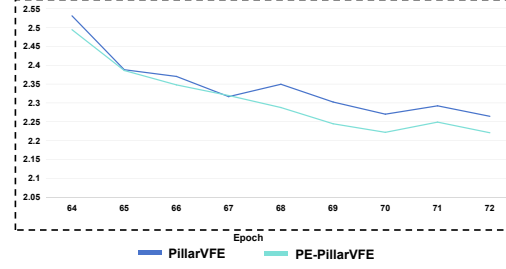


Fig. 4: The loss comparison of different PFE designs.

merical differences between the input data channels without sacrificing the information contained in the point cloud. This design helps the network achieve better optimization results. Furthermore, to demonstrate the effectiveness of our PE-PFE design compared to the naive PFE from PointPillars [18], we present the performance comparison in the Car category. As shown in Table I, our simple yet effective PE-PFE design yields 1.9 point gains in Success and 0.7 point improvement in Precision. As shown in Figure 4, the design of PE-PFE leads to lower loss values, enabling the network to find better parameters and achieve superior performance.

#### B. Modality-aware Transformer-based Backbone

Recent studies [14], [44], [45] have pointed out that the backbone designs commonly employed in image domain [30], [35], [46], [47] are sub-optimal for point cloud or depth images due to significant modality differences between RGB images and LiDAR point clouds. Particularly, backbone design in image domain tends to utilize more block layers in later stages to extract high-level semantic features for perception. For instance, ResNet-50 [30] takes 6 residual blocks in the 3rd stage while the 1st stage uses 3 blocks for feature extraction. Similarly, Swin-Transformer [35] adopts 9 blocks in the 3rd stage while only 1 block is used in the 1st stage. However, we think that these design choices for distributing computations across stages were largely empirical and may not be well-suited for LiDAR point clouds. Unlike RGB images, LiDAR can capture spatial distances and shapes of objects. This means that rich and accurate geometric information of objects is already explicitly encoded in point cloud. Therefore, we assume that instead of allocating excessive computational resources to model object geometries in later stages like ResNet/Swin-Transformer in RGB images, we propose reallocating more computational resources to the early stages to effectively incorporate the geometric information carried by raw point clouds.

To validate the aforementioned hypothesis for transformer-based backbone, we systematically study computation allocation by adjusting the stage compute ratio in the transformer-based backbone of SMAT [16]. It is worth noting that the setting of SMAT has the same depth number as ResNet-50, with a stage compute ratio of [3,4,6,3]. As shown in Table II, we used the SMAT backbone as the baseline and varied the number of depth blocks from 0 to 4 with a stride of 1 in each stage. From the results, we can find that the



TABLE II: Impact of varying block quantities in the four stages of the backbone on the final results. **Bold** denotes the best performance.

Blocks Number	GFLOPs	Success	Precision
[3,4,6,3] (SMAT [16] <sup>4</sup> )	0.37	68.9	79.6
[2,2,6,2]	0.29	25.7	34.9
[1,1,9,1]	0.29	53.1	56.2
[1,1,1,1]	0.14	69.5	80.1
[2,1,1,1]	0.16	70.3	80.6
<b>[3,1,1,1]</b>	<b>0.18(-0.19)</b>	<b>72.1(+3.2)</b>	<b>82.1(+2.5)</b>
[4,1,1,1]	0.21	68.7	78.9
[1,2,1,1]	0.16	70.1	80.7
[1,3,1,1]	0.18	69.7	80.6
[1,4,1,1]	0.20	69.4	79.4
[1,1,2,1]	0.16	68.4	78.8
[1,1,3,1]	0.18	70.0	80.8
[1,1,4,1]	0.20	71.0	81.8
[1,1,1,2]	0.15	68.0	78.3
[1,1,1,3]	0.17	68.1	78.4
[1,1,1,4]	0.18	69.3	80.0

performance is quite sensitive to the capacity of early stage 1, while being less sensitive to the later stages (2, 3, 4). This confirmed that allocating more computational resources to the early stages is beneficial for enabling the network to better capture the geometric information carried by the raw point clouds. Based on this observation, we set the stage compute ratio of the four stages to [3,1,1,1]. It is worth noting that with this depth blocks setting, our modality-aware transformer backbone network achieved promising performance improvements in terms of 3.2 point in Success and 2.5 point in Precision metric, while significantly reducing the computational cost by half the GFLOPs compared to the baseline method (from 0.37 to 0.18).

**Differences with Previous Study.** Our results differ significantly from previous studies [14], [44], which were focused on LiDAR-based object detection tasks using CNN architecture with local receptive fields. In contrast, we focus on 3D SOT tasks within local search area and design a transformer architecture with global receptive fields. Therefore, by allocating more computational resources to the 1st stage, our network is able to capture the enough global-aware geometric information of the input point cloud. This is different with CNN-based backbone, which require more computational resources allocated to both the 1st and 2nd stages. As a result, our modality-aware transformer-based backbone design proves to be more effective.

### C. Activation Function Selection for Point Cloud

$$GeLU(x) = \frac{1}{2}x \left( 1 + \frac{2}{\sqrt{\pi}} \int_0^{\frac{x}{\sqrt{2}}} e^{-\eta^2} d\eta \right) \quad (1)$$

$$ReLU(x) = \max(0, x) \quad (2)$$

$$LeakyReLU(x) = \begin{cases} x & \text{if } x > 0, \\ \alpha x & \text{if } x \leq 0. \end{cases} \quad (3)$$

There is a discrepancy between the choice of activation functions natural language processing (NLP) and vision architectures. Rectified Linear Unit (ReLU) [48] is extensively used in convolutional networks (ConvNets) due to its simplicity and efficiency. With the Transformer [26] merging, Gaussian Error Linear Unit (GELU) [49] is considered as a smoother variant of ReLU and has been employed in state-of-the-art Transformer models, such as Google’s BERT [50], OpenAI’s GPT-3 [51], and Vision Transformers [34], [35], demonstrating superior performance across various language and vision tasks. However, unlike image or text data, point cloud input data contains negative values that represent corresponding geometric property. We assume that directly applying ReLU or GELU activation functions to point clouds would suppress the negative values and result in information loss. To address this issue, we explored the Leaky Rectified Linear Unit (LeakyReLU) [52], which can address the issue of neuron death and preserve more information within the range of values less than zero. As shown in Eq. 1,2,3 The GELU and ReLU functions exhibit saturation behavior when the input values are less than zero, effectively reducing the information content. In contrast, the LeakyReLU function preserves the negative range of input values, enabling the retention of valuable information.

TABLE III: Influence of different activation functions on Car category. **Bold** denotes the best result

PFE Method	Success	Precision
GELU (SMAT [16] <sup>4</sup> )	68.9	79.6
ReLU	69.9	80.7
<b>LeakyReLU</b>	<b>71.2 (+2.3)</b>	<b>81.8 (+2.2)</b>

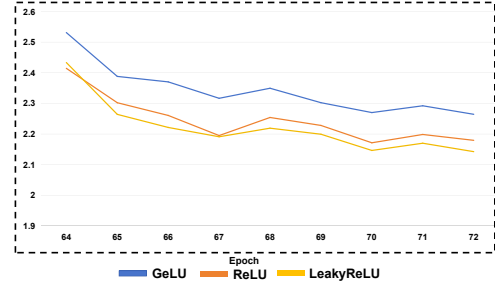


Fig. 5: **The impact of different activation functions on the reduction of the Epoch Loss.** In particular, the LeakyReLU activation function has shown a more pronounced decrease in loss compared to the other two functions under consideration.

Therefore, we simply replace the GeLU activation function in SMAT with LeakyReLU function. As shown in Tab III and Figure 5, using LeakyReLU function has better performance (+2.3 in Success and 2.2 in Precision) and lower loss value than other functions, highlighting the significant impact of activation function choice on 3D single object tracking tasks based on point cloud modality.

## V. EXPERIMENTS

**KITTI Dataset.** We conduct training and evaluating for our task using the KITTI [56] datasets. We follow the

TABLE IV: Overall performance comparison on the KITTI dataset. The best two results are highlighted in red, blue.

Method	Publication	Modality	Paradigm	View	Mean-by class		Mean-by frame	
					Success	Precision	Success	Precision
$M^2$ -Track [21]	CVPR 2022	LIDAR	Motion	Point	61.9	<b>80.2</b>	60.6	<b>80.1</b>
SC3D [10]	CVPR 2019	LIDAR	Similarity	Point	35.4	53.3	31.2	48.5
P2B [2]	CVPR 2020			Point	39.5	53.9	42.4	60.0
3D-SiamRPN [1]	IEEE Sensors J			Point	43.8	58.6	46.6	64.9
MLVSNet [53]	ICCV2021			Point	44.1	60.3	45.7	66.7
BAT [4]	ICCV 2021			Point	47.2	65.1	51.2	72.8
PTT [3]	IROS 2021			Point	48.4	63.4	55.1	74.2
LTTR [5]	BMVC 2021			Voxel	50.0	67.4	48.7	65.8
V2B [22]	NeurIPS 2021			Point+Voxel	52.4	65.6	58.4	75.2
PTTR [6]	CVPR 2022			Point	58.4	77.8	57.9	78.1
CMT [27]	ECCV 2022			Point	57.2	76.0	59.4	77.6
STNet [7]	ECCV 2022			Point	<b>63.4</b>	<b>81.4</b>	<b>61.3</b>	<b>80.1</b>
C2FT [54]	RAL 2022			Point	51.6	67.7	57.2	76.4
MLSET [55]	RAL 2023			Point	54.2	68.9	59.6	78.4
SMAT [16]	RAL 2022			Pillar	56.7	76.1	60.4	79.5
<b>PillarTrack</b>	Ours			Pillar	<b>63.7 +7.0</b>	<b>78.9 +2.8</b>	<b>65.3 +4.9</b>	<b>82.2 +2.7</b>

TABLE V: Detailed per-class performance on the KITTI dataset. The best two results are highlighted in red, blue.

Method	Car-6424		Pedestrian-6088		Van-1248		Cyclist-308	
	Success	Precision	Success	Precision	Success	Precision	Success	Precision
$M^2$ -Track [21]	64.8	79.2	<b>57.6</b>	<b>83.6</b>	50.4	64.8	<b>74.9</b>	93.3
SC3D [10]	41.3	57.9	18.2	37.8	40.4	47.0	41.5	70.4
P2B [2]	56.2	72.8	28.7	49.6	40.8	48.4	32.1	44.7
3D-SiamRPN [1]	58.2	76.2	35.2	56.2	45.7	52.9	36.2	49.0
MLVSNet [53]	56.0	74.0	34.1	61.1	52.0	61.4	34.3	44.5
BAT [4]	60.5	77.7	42.1	70.1	52.4	67.0	33.7	45.4
PTT [3]	67.8	81.8	44.9	72.0	43.6	52.5	37.2	47.3
LTTR [5]	65.0	77.1	33.2	56.8	35.8	45.6	66.2	89.9
V2B [22]	70.5	81.3	48.3	73.5	50.1	58.0	40.8	49.7
PTTR [6]	65.2	77.4	50.9	81.6	52.5	61.8	65.1	90.5
CMT [27]	70.5	81.9	49.1	75.5	54.1	64.1	55.1	82.4
STNet [7]	<b>72.1</b>	<b>84.0</b>	49.9	77.2	<b>58.0</b>	<b>70.6</b>	73.5	<b>93.7</b>
C2FT [54]	67.0	80.4	48.6	75.6	53.4	<b>66.1</b>	38.0	48.7
MLSET [55]	69.7	81.0	50.7	80.0	<b>55.2</b>	64.8	41.0	49.7
SMAT [16]	71.9	82.4	52.1	81.5	41.4	53.2	61.2	87.3
<b>PillarTrack (Ours)</b>	<b>74.2 +2.3</b>	<b>85.1 +2.7</b>	<b>59.7+7.6</b>	<b>84.7 +3.2</b>	43.4 +2.0	51.7 –	<b>77.4 +16.2</b>	<b>94.2 +6.9</b>

same setting in baseline model [16] to divide the sequences into training, validation, and testing splits, where 0-16 for training, 17-18 for validation and 19-20 for testing.

**NuScenes Dataset.** The NuScenes [57] dataset comprises 1000 scenes, which are allocated into 700/150/150 scenes for training, validation, and testing, respectively. Each scene is populated with approximately 300,000 points and is accompanied by comprehensive 360-degree viewpoint annotations. In our research, we adhere to the dataset configuration established by Open3DSOT [21] for the training and evaluation of our methodology. We also conduct a comparative analysis with the baseline model [16] to evaluate the efficacy and superiority of our designs.

**Evaluation metrics.** We use One-Pass Evaluation (OPE) [58] to measure Success and Precision. The Success measure the 3D IoU between the predicted box and the ground truth box, the Precision measures the AUC of the distance error between the center of the predicted and ground truth box.

**Implementation details.** We follow our baseline model

[16] and employ PVTv2-b2 [37] as backbone, adhering to its original configuration. The specific settings include a head number of [1, 2, 5, 8], a depth configuration of [3, 1, 1, 1], the expansion ratio for the feed-forward layer set to [8, 8, 4, 8] and a channel number configuration of [64, 128, 320, 512]. In KITTI dataset, we set [0.1, 0.1, 4] meters as pillar size and a search area of [-3.2, -3.2, -3, 3.2, 3.2, 1] meters for the car category. In nuScenes dataset, we set [0.075, 0.075, 8] meters as pillar size and a search area of [-3.2, -3.2, -5, 3.2, 3.2, 3] meters for the car category. Additionally, the LeakyReLU activation is employed with a negative slope value of 0.01.

**Training details.** On the KITTI dataset, we train PillarTrack with AdamW [59] optimizer with an initial learning rate of 0.0001, a weight decay of 0.05, and a batch size of 16 on a NVIDIA 3090 GPU. The total number of training epochs was set to 72. For the NuScenes dataset, the training was conducted over 18 epochs, with a learning rate decay by a factor of 10 at epoch 14.

Method	Paradigm	Car-64159		Pedestrian-33227		Truck-13587		Trailer-3352		Bus-2953		Mean by class		Mean by frame	
		Success	Precision	Success	Precision	Success	Precision	Success	Precision	Success	Precision	Success	Precision	Success	Precision
<i>M<sup>2</sup></i> -Tracker [21]	Motion	<b>55.85</b>	<b>65.09</b>	32.10	<b>60.92</b>	<b>57.36</b>	<b>59.54</b>	<b>57.61</b>	<b>58.26</b>	<b>51.39</b>	<b>51.44</b>	<b>50.86</b>	<b>59.05</b>	<b>49.23</b>	<b>62.73</b>
SC3D [10]	Similarity	22.31	21.93	11.29	12.65	30.67	27.73	35.28	28.12	29.35	24.08	25.78	22.90	20.70	20.20
P2B [2]		38.81	43.18	28.39	52.24	42.95	41.59	48.96	40.05	32.95	27.41	38.41	40.90	36.48	45.08
PTT [12]		41.22	45.26	19.33	32.03	50.23	48.56	51.70	46.50	39.40	36.70	40.38	41.81	36.33	41.72
BAT [4]		40.73	43.29	28.83	53.32	45.34	42.58	52.59	44.89	35.44	28.01	40.59	42.42	38.10	45.71
GLT-T [60]		48.52	54.29	31.74	56.49	52.74	51.43	57.60	52.01	44.55	40.69	47.03	50.98	44.42	54.33
PTTR [6]		<b>51.89</b>	<b>58.61</b>	29.90	45.09	45.30	44.74	45.87	38.36	43.14	37.74	43.22	44.91	44.50	52.07
SMAT [16]		43.51	49.04	<b>32.27</b>	60.28	44.78	44.69	37.45	34.10	39.42	34.32	39.49	44.49	40.20	50.92
<b>PillarTrack</b>		47.12	57.72	<b>34.18</b>	<b>64.93</b>	<b>54.82</b>	<b>54.41</b>	<b>57.70</b>	<b>54.63</b>	<b>44.68</b>	<b>40.73</b>	<b>47.70</b>	<b>54.48</b>	<b>44.59</b>	<b>58.86</b>
Improvement		<b>+3.61</b>	<b>+8.68</b>	<b>+1.91</b>	<b>+4.65</b>	<b>+10.04</b>	<b>+9.72</b>	<b>+17.25</b>	<b>+20.53</b>	<b>+5.26</b>	<b>+6.41</b>	<b>+8.21</b>	<b>+9.99</b>	<b>+4.39</b>	<b>+7.94</b>

TABLE VI: Performance comparison on the NuScenes dataset. The best two results are highlighted in red, blue.

#### A. Quantitative results on KITTI.

As shown in Table IV and V, the proposed PillarTrack demonstrates significant performance improvements compared to the baseline method (SMAT [16]). Specifically, PillarTrack achieved a performance improvement of 7.0% 2.8% and 4.9% 2.7% in Success and Precision metrics in terms of mean by-class and mean-by frame setting, respectively.

In the categories of the Car, Pedestrian, Van, and Cyclist, PillarTrack outperformed SMAT by 2.3%, 7.6%, 2.0%, and 16.2% in Success, respectively. These improvements can be attributed to the effective designs of PillarTrack. Firstly, PE-PFE module could stabilize network training without information loss. Secondly, the modality-aware transformer-based backbone focuses on capturing more geometric information from point clouds and enhance the feature representation capability of pillars. Lastly, LeakyReLU activation retains more information and help network optimization. Besides, PillarTrack also surpassed the motion-based method MM-Track [21] in the categories of Car, Pedestrian, and Cyclist, achieving state-of-the-art performance on the KITTI dataset. However, for Van, our method only has 43.4% in Success. We believe there are two main reasons for this. Firstly, the point clouds of vans are concentrated on the object surfaces, and after pillar encoding, they lack distinctive geometric features, making them more challenging to track accurately. Secondly, the limited number of training samples for the Van category may have constrained the model’s performance, as it might not have captured the full range of variations and characteristics exhibited by vans in the real world.

#### B. Quantitative results on NuScenes.

As illustrated in Table VI, our PillarTrack achieves the second-best performance across the five categories on the nuScenes dataset. Compared to previous methods, M2-Tracker [21] adopts a different motion-based paradigm for object tracking, demonstrating superior results compared to the similarity-based paradigm. Meanwhile, our PillarTrack attains the best results among the similarity-based methods. Furthermore, compared to the baseline method [16], PillarTrack has demonstrated significant improvements in each category. Specifically, PillarTrack has enhanced the mean class-wise and frame-wise Success and Precision metrics by 8.21% / 9.99% and 4.39% / 7.94%, respectively. In terms of Success for each category, PillarTrack achieves notable improvements of 3.61% for Car, 1.91% for Pedestrian,

10.04% for Truck, 17.25% for Trailer, and 5.26% for Bus. Importantly, the Truck and Trailer categories demonstrate significantly enhanced performance compared to baseline. However, such improvements were not observed in the Van category in the KITTI dataset. We attribute this to two reasons: (1) The KITTI dataset only provides front-view annotations. Under the front-view perspective, the model is constrained to learn feature representations specific to the truck from a single viewpoint, which limits the acquisition of comprehensive geometric information about the Van. As a result, the Siamese network based on appearance matching struggles to capture the key geometric information of the Van. Conversely, the NuScenes dataset provides 360-degree surround view point cloud data with corresponding annotations. This enables superior learning of both appearance and geometric representations, leading to significant performance enhancement by effectively utilizing multi-view point cloud data. (2) The KITTI dataset contains a limited number of annotated van samples (1248), whereas the NuScenes dataset offers a larger sample size (13587/3352). Within our effective framework design, this facilitates richer feature representation learning, leading to performance improvements. Besides, our performance is slightly lower than that of PTTR on Car category. We think this is because PTTR utilizes both point-based and pillar-based representations to encode the input point cloud, resulting in superior performance, particularly in terms of the Success metric.

#### C. Visualization results.

To comprehensively evaluate the performance of our method, particularly its capability to handle point clouds of varying sparsity, we conduct visualization on the different category, encompassing both sparse and dense scenes. Through comparative experiments on the initial frame and subsequent sequences, our method demonstrated superior tracking accuracy in both sparse and dense point cloud environments compared to the baseline SMAT method, highlighting ours enhanced adaptability and robustness. In the Cyclist category, our method was able to consistently track the target, whereas SMAT occasionally lost the target. For the Pedestrian category, our method maintained stable tracking from the outset, while SMAT failed to accurately identify the target initially. The visualization results in Figure 5 further substantiate the effectiveness and superior performance of our method across various scenarios.

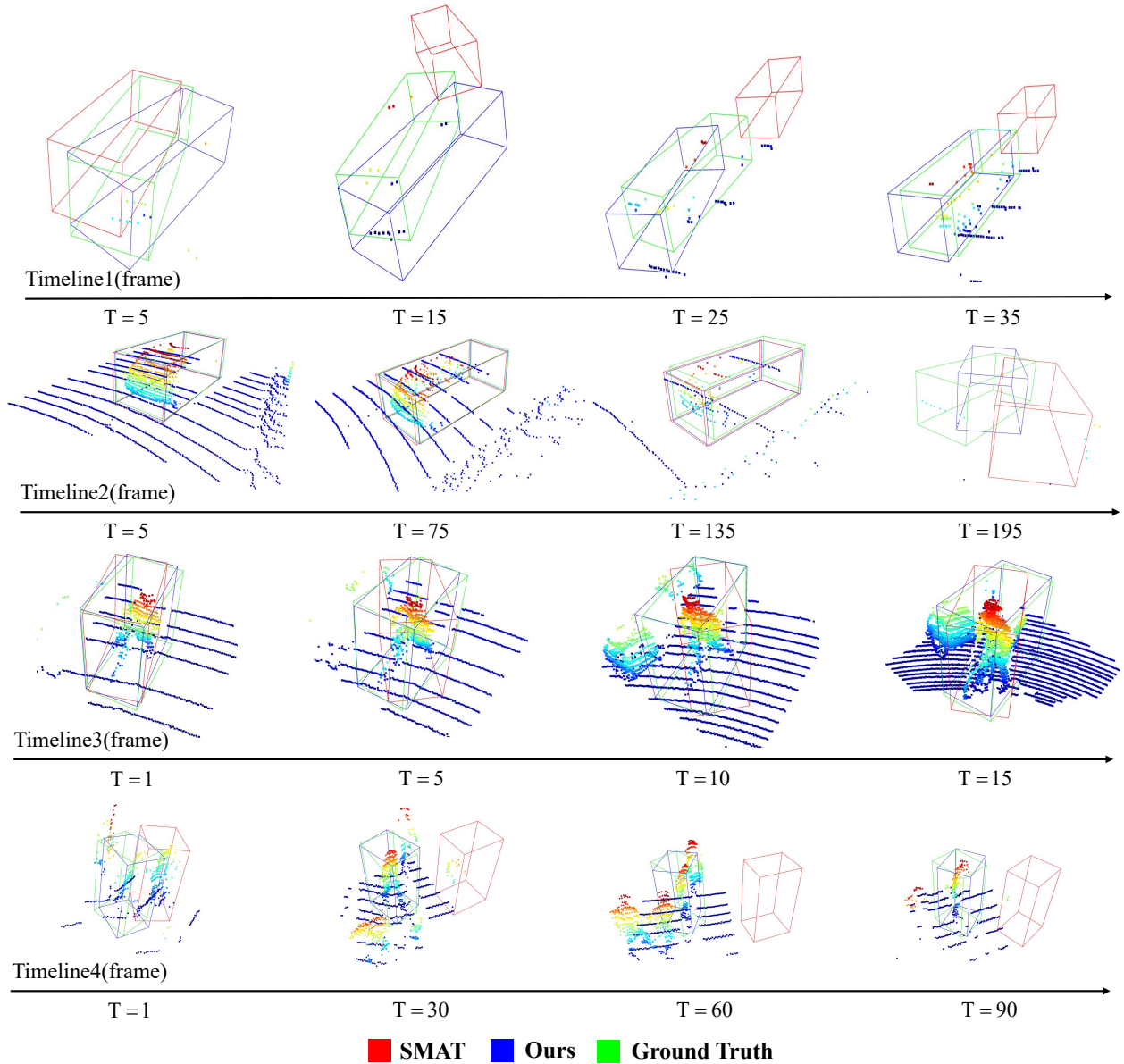


Fig. 6: Visualization results comparison of our PillarTrack and baseline method (SMAT [16]) on the categories of Car, Pedestrian and Cyclist in KITTI dataset.

#### D. Running Speed

We calculated the average running time of all test frames for car to measure PillarTrack’s speed. PillarTrack model achieved 27 FPS on a single NVIDIA 3080 GPU, while baseline model SMAT has a 18.2 FPS in the inference phase. We did not introduce extra computational parameters, and we further reduced the computational overhead on the backbone while increasing the model’s performance. This once again demonstrates the effectiveness of our PillarTrack. Furthermore, our proposed PillarTrack can leverage quantization techniques [61], [62] to accelerate the runtime. We leave this problem for future research.

## VI. CONCLUSIONS

In this work, we proposed PillarTrack, a pillar-based 3D single-object tracking framework that decreases computation overhead while improving performance. The framework introduces a Pyramid-type Encoding Pillar Feature Encoder (PE-PFE) and a modality-aware Transformer-based backbone, and a simply replacement of activation function. Our extensive experiments on the KITTI dataset demonstrate PillarTrack’s superior performance, achieving a better trade-off between speed and accuracy. Based on above designs and its efficiency, We hope to inspire the community to rethink the design of network for 3D single object tracking based on point clouds.



## REFERENCES

- [1] Z. Fang, S. Zhou, Y. Cui, and S. Scherer, "3d-siamrpn: An end-to-end learning method for real-time 3d single object tracking using raw point cloud," *IEEE Sensors Journal*, vol. 21, no. 4, pp. 4995–5011, 2020.
- [2] H. Qi, C. Feng, Z. Cao, F. Zhao, and Y. Xiao, "P2b: Point-to-box network for 3d object tracking in point clouds," in *Proceedings of the IEEE/CVF conference on computer vision and pattern recognition*, pp. 6329–6338, 2020.
- [3] J. Shan, S. Zhou, Z. Fang, and Y. Cui, "Ptt: Point-track-transformer module for 3d single object tracking in point clouds," in *2021 IEEE/RSJ International Conference on Intelligent Robots and Systems (IROS)*, pp. 1310–1316, IEEE, 2021.
- [4] C. Zheng, X. Yan, J. Gao, W. Zhao, W. Zhang, Z. Li, and S. Cui, "Box-aware feature enhancement for single object tracking on point clouds," in *International Conference on Computer Vision*, pp. 13199–13208, 2021.
- [5] Y. Cui, Z. Fang, J. Shan, Z. Gu, and S. Zhou, "3d object tracking with transformer," in *The British Machine Vision Conference*, 2021.
- [6] C. Zhou, Z. Luo, Y. Luo, T. Liu, L. Pan, Z. Cai, H. Zhao, and S. Lu, "Ptr: Relational 3d point cloud object tracking with transformer," in *Computer Vision and Pattern Recognition*, pp. 8531–8540, 2022.
- [7] L. Hui, L. Wang, L. Tang, K. Lan, J. Xie, and J. Yang, "3d siamese transformer network for single object tracking on point clouds," in *ECCV*, 2022.
- [8] C. R. Qi, H. Su, K. Mo, and L. J. Guibas, "Pointnet: Deep learning on point sets for 3D classification and segmentation," in *CVPR*, pp. 652–660, 2017.
- [9] C. R. Qi, L. Yi, H. Su, and L. J. Guibas, "Pointnet++: Deep hierarchical feature learning on point sets in a metric space," in *NeurIPS*, pp. 5099–5108, 2017.
- [10] S. Giancola, J. Zarzar, and B. Ghanem, "Leveraging shape completion for 3d siamese tracking," in *Proceedings of the IEEE/CVF conference on computer vision and pattern recognition*, pp. 1359–1368, 2019.
- [11] C. R. Qi, H. Su, K. Mo, and L. J. Guibas, "Pointnet: Deep learning on point sets for 3d classification and segmentation," in *Proceedings of the IEEE conference on computer vision and pattern recognition*, pp. 652–660, 2017.
- [12] S. Jiayao, S. Zhou, Y. Cui, and Z. Fang, "Real-time 3d single object tracking with transformer," *IEEE Transactions on Multimedia*, pp. 1–1, 2022.
- [13] G. Shi, R. Li, and C. Ma, "Pillarnet: Real-time and high-performance pillar-based 3d object detection," in *ECCV*, 2022.
- [14] S. Zhou, Z. Tian, X. Chu, X. Zhang, B. Zhang, X. Lu, C. Feng, Z. Jie, P. Y. Chiang, and L. Ma, "Fastpillars: A deployment-friendly pillar-based 3d detector," *arXiv preprint arXiv:2302.02367*, 2023.
- [15] J. Li, C. Luo, and X. Yang, "Pillarnet: Rethinking network designs for 3d object detection in lidar point clouds," in *Computer Vision and Pattern Recognition (CVPR)*, 2023.
- [16] Y. Cui, J. Shan, Z. Gu, Z. Li, and Z. Fang, "Exploiting more information in sparse point cloud for 3d single object tracking," *IEEE Robotics and Automation Letters*, vol. 7, no. 4, pp. 11926–11933, 2022.
- [17] Z. Luo, C. Zhou, L. Pan, G. Zhang, T. Liu, Y. Luo, H. Zhao, Z. Liu, and S. Lu, "Exploring point-bev fusion for 3d point cloud object tracking with transformer," *IEEE transactions on pattern analysis and machine intelligence*, 2024.
- [18] A. H. Lang, S. Vora, H. Caesar, L. Zhou, J. Yang, and O. Beijbom, "Pointpillars: Fast encoders for object detection from point clouds," in *Proceedings of the IEEE/CVF conference on computer vision and pattern recognition*, pp. 12697–12705, 2019.
- [19] Y. Cui, Z. Fang, and S. Zhou, "Point siamese network for person tracking using 3d point clouds," *Sensors*, vol. 20, no. 1, p. 143, 2019.
- [20] H. Zou, J. Cui, X. Kong, C. Zhang, Y. Liu, F. Wen, and W. Li, "F-siamese tracker: A frustum-based double siamese network for 3d single object tracking," *2020 IEEE/RSJ International Conference on Intelligent Robots and Systems (IROS)*, pp. 8133–8139, 2020.
- [21] C. Zheng, X. Yan, H. Zhang, B. Wang, S. Cheng, S. Cui, and Z. Li, "Beyond 3d siamese tracking: A motion-centric paradigm for 3d single object tracking in point clouds," in *Proceedings of the IEEE/CVF Conference on Computer Vision and Pattern Recognition*, pp. 8111–8120, 2022.
- [22] L. Hui, L. Wang, M. Cheng, J. Xie, and J. Yang, "3d siamese voxel-to-bev tracker for sparse point clouds," *Advances in Neural Information Processing Systems*, vol. 34, pp. 28714–28727, 2021.
- [23] L. Bertinetto, J. Valmadre, J. F. Henriques, A. Vedaldi, and P. H. Torr, "Fully-convolutional siamese networks for object tracking," in *Computer Vision—ECCV 2016 Workshops: Amsterdam, The Netherlands, October 8–10 and 15–16, 2016, Proceedings, Part II 14*, pp. 850–865, Springer, 2016.
- [24] C. R. Qi, O. Litany, K. He, and L. J. Guibas, "Deep hough voting for 3d object detection in point clouds," in *ICCV*, pp. 9277–9286, 2019.
- [25] C. Zheng, X. Yan, H. Zhang, B. Wang, S. Cheng, S. Cui, and Z. Li, "An effective motion-centric paradigm for 3d single object tracking in point clouds," *arXiv preprint arXiv:2303.12535*, 2023.
- [26] A. Vaswani, N. Shazeer, N. Parmar, J. Uszkoreit, L. Jones, A. N. Gomez, Ł. Kaiser, and I. Polosukhin, "Attention is all you need," *Advances in neural information processing systems*, vol. 30, 2017.
- [27] Z. Guo, Y. Mao, W. Zhou, M. Wang, and H. Li, "Cmt: Context-matching-guided transformer for 3d tracking in point clouds," in *European Conference on Computer Vision*, pp. 95–111, Springer, 2022.
- [28] K. Lan, H. Jiang, and J. Xie, "Temporal-aware siamese tracker: Integrate temporal context for 3d object tracking," in *Proceedings of the Asian Conference on Computer Vision*, pp. 399–414, 2022.
- [29] T.-X. Xu, Y.-C. Guo, Y.-K. Lai, and S.-H. Zhang, "Cttrack: Improving 3d point cloud tracking with contextual information," in *Proceedings of the IEEE/CVF Conference on Computer Vision and Pattern Recognition*, pp. 1084–1093, 2023.
- [30] K. He, X. Zhang, S. Ren, and J. Sun, "Deep residual learning for image recognition," in *Proceedings of the IEEE conference on computer vision and pattern recognition*, pp. 770–778, 2016.
- [31] T. Yin, X. Zhou, and P. Krahenbuhl, "Center-based 3d object detection and tracking," in *Proceedings of the IEEE/CVF conference on computer vision and pattern recognition*, pp. 11784–11793, 2021.
- [32] Y. Zhou and O. Tuzel, "Voxelnet: End-to-end learning for point cloud based 3d object detection," in *Proceedings of the IEEE conference on computer vision and pattern recognition*, pp. 4490–4499, 2018.
- [33] Y. Yan, Y. Mao, and B. Li, "Second: Sparsely embedded convolutional detection," *Sensors*, vol. 18, no. 10, p. 3337, 2018.
- [34] A. Dosovitskiy, L. Beyer, A. Kolesnikov, D. Weissenborn, X. Zhai, T. Unterthiner, M. Dehghani, M. Minderer, G. Heigold, S. Gelly, *et al.*, "An image is worth 16x16 words: Transformers for image recognition at scale," *arXiv preprint arXiv:2010.11929*, 2020.
- [35] Z. Liu, Y. Lin, Y. Cao, H. Hu, Y. Wei, Z. Zhang, S. Lin, and B. Guo, "Swin transformer: Hierarchical vision transformer using shifted windows," 2021.
- [36] W. Wang, E. Xie, X. Li, D.-P. Fan, K. Song, D. Liang, T. Lu, P. Luo, and L. Shao, "Pyramid vision transformer: A versatile backbone for dense prediction without convolutions," in *Proceedings of the IEEE/CVF international conference on computer vision*, pp. 568–578, 2021.
- [37] W. Wang, E. Xie, X. Li, D.-P. Fan, K. Song, D. Liang, T. Lu, P. Luo, and L. Shao, "Pvt v2: Improved baselines with pyramid vision transformer," *Computational Visual Media*, vol. 8, no. 3, pp. 415–424, 2022.
- [38] H. Zhao, L. Jiang, J. Jia, P. H. Torr, and V. Koltun, "Point transformer," in *Proceedings of the IEEE/CVF international conference on computer vision*, pp. 16259–16268, 2021.
- [39] M.-H. Guo, J.-X. Cai, Z.-N. Liu, T.-J. Mu, R. R. Martin, and S.-M. Hu, "Pct: Point cloud transformer," *Computational Visual Media*, vol. 7, pp. 187–199, 2021.
- [40] L. Fan, Z. Pang, T. Zhang, Y.-X. Wang, H. Zhao, F. Wang, N. Wang, and Z. Zhang, "Embracing single stride 3d object detector with sparse transformer," in *Proceedings of the IEEE/CVF conference on computer vision and pattern recognition*, pp. 8458–8468, 2022.
- [41] Z. Liu, X. Yang, H. Tang, S. Yang, and S. Han, "Flatformer: Flattened window attention for efficient point cloud transformer," in *Proceedings of the IEEE/CVF Conference on Computer Vision and Pattern Recognition*, pp. 1200–1211, 2023.
- [42] X. Glorot and Y. Bengio, "Understanding the difficulty of training deep feedforward neural networks," in *Proceedings of the thirteenth international conference on artificial intelligence and statistics*, pp. 249–256, JMLR Workshop and Conference Proceedings, 2010.
- [43] S. Santurkar, D. Tsipras, A. Ilyas, and A. Madry, "How does batch normalization help optimization?," *Advances in neural information processing systems*, vol. 31, 2018.
- [44] Z. Tian, X. Chu, X. Wang, X. Wei, and C. Shen, "Fully convolutional one-stage 3d object detection on lidar range images," *NeurIPS*, 2022.

- [45] J. Shang and S. Zhou, "Lk-unet: Large kernel design for 3d medical image segmentation," in *ICASSP 2024 - 2024 IEEE International Conference on Acoustics, Speech and Signal Processing (ICASSP)*, pp. 1576–1580, 2024.
- [46] K. Simonyan and A. Zisserman, "Very deep convolutional networks for large-scale image recognition," *arXiv preprint arXiv:1409.1556*, 2014.
- [47] Z. Liu, H. Mao, C.-Y. Wu, C. Feichtenhofer, T. Darrell, and S. Xie, "A convnet for the 2020s," in *Proceedings of the IEEE/CVF conference on computer vision and pattern recognition*, pp. 11976–11986, 2022.
- [48] A. F. Agarap, "Deep learning using rectified linear units (relu)," *arXiv preprint arXiv:1803.08375*, 2018.
- [49] D. Hendrycks and K. Gimpel, "Gaussian error linear units (gelu)," *arXiv preprint arXiv:1606.08415*, 2016.
- [50] J. Devlin, M.-W. Chang, K. Lee, and K. Toutanova, "Bert: Pre-training of deep bidirectional transformers for language understanding," *arXiv preprint arXiv:1810.04805*, 2018.
- [51] T. Brown, B. Mann, and N. Ryder, "Language models are few-shot learners," *Advances in neural information processing systems*, vol. 33, pp. 1877–1901, 2020.
- [52] A. L. Maas, A. Y. Hannun, A. Y. Ng, *et al.*, "Rectifier nonlinearities improve neural network acoustic models," in *Proc. icml*, vol. 30, p. 3, Atlanta, GA, 2013.
- [53] Z. Wang, Q. Xie, Y.-K. Lai, J. Wu, K. Long, and J. Wang, "Mlvs-net: Multi-level voting siamese network for 3d visual tracking," in *Proceedings of the IEEE/CVF International Conference on Computer Vision (ICCV)*, pp. 3101–3110, October 2021.
- [54] B. Fan, K. Wang, H. Zhang, and J. Tian, "Accurate 3d single object tracker with local-to-global feature refinement," *IEEE Robotics and Automation Letters*, vol. 7, no. 4, pp. 12211–12218, 2022.
- [55] Q. Wu, C. Sun, and J. Wang, "Multi-level structure-enhanced network for 3d single object tracking in sparse point clouds," *IEEE Robotics and Automation Letters*, vol. 8, no. 1, pp. 9–16, 2022.
- [56] A. Geiger, P. Lenz, and R. Urtasun, "Are we ready for autonomous driving? the kitti vision benchmark suite," in *2012 IEEE conference on computer vision and pattern recognition*, pp. 3354–3361, IEEE, 2012.
- [57] H. Caesar, V. Bankiti, A. H. Lang, S. Vora, V. E. Liong, Q. Xu, A. Krishnan, Y. Pan, G. Baldan, and O. Beijbom, "nuscenes: A multimodal dataset for autonomous driving," in *Proceedings of the IEEE/CVF conference on computer vision and pattern recognition*, pp. 11621–11631, 2020.
- [58] M. Kristan, J. Matas, A. Leonardis, T. Vojř, R. Pflugfelder, G. Fernandez, G. Nebehay, F. Porikli, and L. Čehovin, "A novel performance evaluation methodology for single-target trackers," *IEEE transactions on pattern analysis and machine intelligence*, vol. 38, no. 11, pp. 2137–2155, 2016.
- [59] I. Loshchilov and F. Hutter, "Decoupled weight decay regularization," *arXiv preprint arXiv:1711.05101*, 2017.
- [60] J. Nie, Z. He, Y. Yang, M. Gao, and J. Zhang, "Glt-t: Global-local transformer voting for 3d single object tracking in point clouds," in *Proceedings of the AAAI Conference on Artificial Intelligence*, vol. 37, pp. 1957–1965, 2023.
- [61] S. Zhou, L. Li, X. Zhang, B. Zhang, S. Bai, M. Sun, Z. Zhao, X. Lu, and X. Chu, "Lidar-ptq: Post-training quantization for point cloud 3d object detection," *International Conference on Learning Representations (ICLR)*, 2024.
- [62] M. Nagel, M. Fournarakis, R. A. Amjad, Y. Bondarenko, M. Van Baalen, and T. Blankevoort, "A white paper on neural network quantization," *arXiv preprint arXiv:2106.08295*, 2021.